ACS OMEGA

http://pubs.acs.org/journal/acsodf

Article

# Effect of Ru Doping on the Properties of $LiFePO_4$/C Cathode Materials for Lithium-Ion Batteries

Yuan Gao,* Kun Xiong, Haidong Zhang, and Bingfeng Zhu*

Cite This: *ACS Omega* 2021, 6, 14122−14129

Read Online

ACCESS | Metrics & More | Article Recommendations

**ABSTRACT:** Doping of metals is highly effective in improving electrochemical performance of lithium iron phosphate. Here, based on a first-principles calculation result that Ru doping at the Fe sites has positive effects on promoting the ability of electron and $Li^+$ transmission by reducing the lattice parameter and band gap, as well as the increase in Fermi energy, we constructed Ru-doped $LiFe_{1-x}Ru_xPO_4$/C through the sol−gel preparation technology as cathode materials for Li-ion batteries. As a result, LFP-1 ($x$ = 0.01) delivers excellent specific capacities of 162.6 and 110.6 mA h $g^{-1}$ under 0.1 and 10 C, respectively. At the same time, LFP-1 emerges with excellent cycling performance, with a capacity retention of up to 95.6% after 300 cycles at 5 C. Ru doping is beneficial for improving the lithium diffusion coefficient and electrical conductivity, therefore strongly increasing electrochemical performance. This work represents a significant addition to exploring a new class of lithium iron phosphates with excellent performance in new energy storage and transition systems.

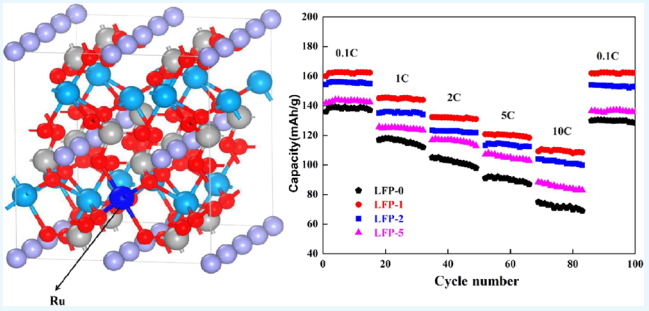


## 1. INTRODUCTION

In recent years, lithium iron phosphate ($LiFePO_4$) has become the highly anticipated commercial positive materials for Li-ion batteries because of a reasonable energy value, low price, high safety, and nontoxic elements.[1−5] Unfortunately, the inferior electronic conductivity and poor lithium-ion transmission capability strongly impede the commercial development for a high-energy-density battery.[6−8] Researchers have carried out various aspects of work to solve these hard problems.[9−18] In these modification methods, improving the intrinsic conductivity of $LiFePO_4$ is still the key problem. The doping of metals is highly effective in improving the intrinsic conductivity of $LiFePO_4$.[19−21]

The electronic conductivity of $LiFePO_4$ is closely related to its microstructure and electronic energy. DFT calculations have made some progress, such as investigating the electronic structure, band structure, surface, and lattice dynamics of cathode materials.[22−25] Ban et al.[26] carried out systematic theoretical calculation and experimental research on $LiFePO_4$, which proved that donor−acceptor charge compensation codoping can significantly improve the material rate capability. Studies reported that the band gap energy can be reduced by doping metal elements to occupy iron or lithium sites, which can effectively enhance the conductivity of $LiFePO_4$.[27] At present, research studies on the doping mechanism mainly focus on the doping of $Co^{2+}$, $Zr^{4+}$, $Nb^{5+}$, $Cr^{3+}$, etc. Due to the similar electronic structure and ionic radius, Ru doping is more likely to occupy the iron site, and the Ru heteroatom substitutes for Fe, in which case, Fe or Li vacancies will be formed in the $LiFePO_4$ lattice to supplement the charge after doping, but the mechanism of high-conductivity Ru doping of $LiFePO_4$ is rarely reported.

In this paper, we first calculated the local crystallographic structure and electronic structure of $LiFe_{1-x}Ru_xPO_4$/C with Ru substituted for Fe by first-principles DFT and then analyzed the effects of Ru doping on the cell parameters, energy band structures, and density of states of $LiFePO_4$ and proposed the change in the mechanism of the conductivity. Above all, our research results proved that raised electronic conductivity and the lithium diffusion coefficient are achieved with Ru doping, thus improving the poor rate performance of $LiFePO_4$ cathode materials in strong current density.

## 2. RESULTS AND DISCUSSION

**2.1. First-Principles Calculations of $LiFe_{1-x}Ru_xPO_4$ Power.** Lattice parameters and Fermi energies of optimized $LiFe_{1-x}Ru_xPO_4$ ($x$ = 0, 0.01, 0.02, and 0.05) from the first-principles calculations are shown in Table 1. It can be seen

Received: February 2, 2021
Accepted: May 13, 2021
Published: May 25, 2021

**Table 1. Unit Cell Parameter and Fermi Energies of Optimized $LiFe_{1-x}Ru_xPO_4$**

| model | $a$ (Å) | $b$ (Å) | $c$ (Å) | $V$ (Å$^3$) | Fermi energy (eV) |
|---|---|---|---|---|---|
| LFP-0 | 10.1283 | 5.9958 | 4.6941 | 285.06 | 3.37 |
| LFP-1 | 10.0508 | 5.9621 | 4.6999 | 281.64 | 3.52 |
| LFP-2 | 9.9921 | 5.9145 | 4.7108 | 278.40 | 3.47 |
| LFP-5 | 9.9833 | 5.8345 | 4.7178 | 274.80 | 3.33 |

from Table 1 that parameters $a$ and $b$ significantly reduce in pace with an increase in the Ru-doped content. In the meantime, unit cell parameter $c$ shows a small raise. These changes lead to the contraction of the unit cell volume. Compression of lattice parameters may come from the smaller radius of Ru (0.68 Å) compared with Fe (0.78 Å). The decrease in lattice parameter $b$ on the Ru-doped LFP can shorten the movement path of $Li^+$ in the [010] direction and enhance $Li^+$ diffusion in the bulk phase.[28,29] At the same time, the decrease in parameter $a$ and the increase in parameter $c$ are beneficial for decreasing the diffusion energy of $Li^+$.

In addition, Table 1 shows that Fermi energy increases from 3.37 to 3.51 eV, when Ru doping increases to 0.01. It can be inferred that doping a small amount of Ru will increase the average voltage of $LiFePO_4$, thus increasing the energy density, which is consistent with the experimental results reported in ref 30. However, with the further increases in the Ru doping amount, Fermi energy decreases gradually. When the doping amounts are 0.02 and 0.05, the Fermi energies are 3.47 and 3.33 eV, respectively. The enhancement of Fermi energy is possibly attributed to the increase in the number of d orbital electrons after Ru doping in Fe sites, which is important in electron transport. Excessive doping of Ru could lead to local lattice distortion and influence the electronic states of the system, causing Fermi energy to decrease.

Figure 1 exhibits the XRD test results of unmodified and Ru-modified $LiFe_{1-x}Ru_xPO_4$ composites by the sol−gel method.

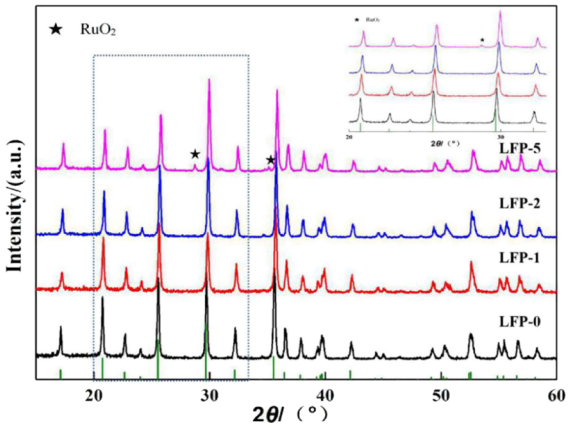


**Figure 1.** X-ray diffraction pattern of $LiFe_{1-x}Ru_xPO_4/C$ ($x$ = 0, 0.01, 0.02, and 0.05). The illustration shows diffraction peaks shift from 20 to 35°.

Four samples have good crystallinity and are very consistent with the standard olivine structure (JCPDS no. 40-1499). This indicates that low doping of Ru does not transform the ordered olivine structure of $LiFePO_4$. With the increase in the Ru content to 0.05, $RuO_2$ ($2\theta$ = 28.72 and 35.11°) as impurity phases comes into being. This implies that the excess doping of Ru does not enter the unit cell of $LiFePO_4$ and forms a separate phase, resulting in the declined electrochemical properties. In addition, as shown in the inset of Figure 1, the peak position moves to a high angle direction regularly, in pace with the increasing doping amount, which indicates a contraction of the unit cell volume. The experimental results are in agreement with the theoretical calculation. It also suggests that Ru doping tends to replace Fe in $LiFePO_4$.

Figure 2 shows the band structures of doped and undoped $LiFePO_4$, which are along the high symmetry point across the first Brillouin zone. Pure $LiFePO_4$ has a high band gap energy of 0.771 eV. The whole energy band is also in the high-energy position. Therefore, $LiFePO_4$ possesses low conductivity. Theoretical analysis indicates that Ru doping is effective in reducing the band gap. The decrease in the band gap of LFP-5 ($x$ = 0.05) is obvious, which is 0.582 eV. The smaller band gap implies higher electrical conductivity, and Ru doping can effectively improve the electronic conductivity of $LiFePO_4$ composite cathode materials.

For clarifying the principle of Ru doping affecting the band structure, the theoretical calculation results of density of states (DOS) of $LiFe_{1-x}Ru_xPO_4$ ($x$ = 0, 0.01, 0.02, and 0.05) samples are discussed and shown in Figure 3. Since the electronic states around the Fermi level have great influence on the electron transfer process, the DOS near the Fermi level has attracted much attention. It is found that the total density of states (TDOS) of cathode materials close to the Fermi level improves with the increase in the Ru doping content, and the peak of the density of states moves toward the low-energy direction, indicating that the band gap decreases after doping. As we know, the Ru $4d^7$ orbit is near the Fermi level, and Ru $4d^7$ also affects the electronic states of $LiFe_{1-x}Ru_xPO_4$ materials just like Fe $3d^6$, which strengthen the peak intensity of $LiFe_{1-x}Ru_xPO_4$ near the Fermi level. Results of DOS theoretical calculation prove that the band gap energy of $LiFe_{1-x}Ru_xPO_4$ can be greatly reduced by Ru doping, which leads to the improvement of conductivity of $LiFe_{1-x}Ru_xPO_4$.

**2.2. Electrochemical Measurements.** Under guidance of theoretical calculation results, electrochemical properties of Ru-doped samples between 4.2 and 2.5 V at 0.1 C were investigated, and test results are shown in Figure 4a. Compared with the $LiFePO_4/C$, Ru doping of $LiFe_{1-x}Ru_xPO_4/C$ exhibits a higher discharge capacity at the first charge−discharge. The LFP-1 ($x$ = 0.01) cathode delivers a specific discharge capacity of 162.6 mA h $g^{-1}$ and discharge plateaus, suggesting the lower polarization and an excellent electrochemical reversibility of the electrode. With the increasing Ru doping amount, discharge capacities of LFP-2 ($x$ = 0.02) and LFP-5 ($x$ = 0.05) are reduced to 156 and 144 mA h $g^{-1}$, respectively, and discharge plateaus decline.

Figure 4b displays cyclic reversibility of $LiFe_{1-x}Ru_xPO_4/C$ electrodes at various rates. All Ru-doped samples show a better rate capability and good cycling characteristics, with no significant decrease in capacity. Apparently, LFP-1 ($x$ = 0.01) shows an outstanding specific capacity and rate capability. LFP-1 delivers specific discharge capacities of 162.6, 145.5, 132.4, 120.0, and 110.6 mA h $g^{-1}$ under different current densities (0.1, 1, 2, 5, and 10 C). After 15 times of charging−discharging, the capacity fading of LFP-1 is very small, and the capacity retention is still higher than 97% at a high rate.

On the contrary, the LFP-0 electrode displays inferior rate performances, and discharge capacities decrease sharply to 75 mA h $g^{-1}$ under 10 C. In addition, the as-prepared LFP-1 ($x$ =


https://doi.org/10.1021/acsomega.1c00595
ACS Omega 2021, 6, 14122−14129

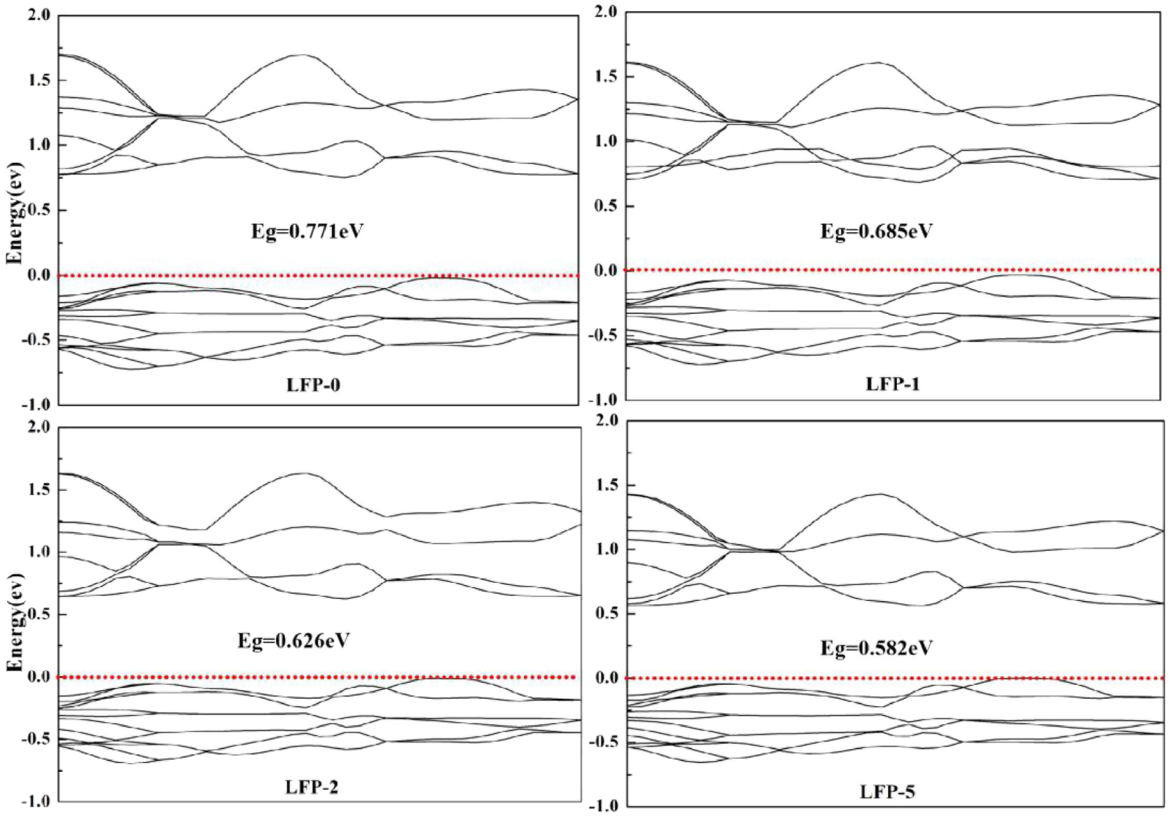


**Figure 2.** Band structures of $LiFe_{1-x}Ru_xPO_4$ ($x$ = 0, 0.01, 0.02, and 0.05).

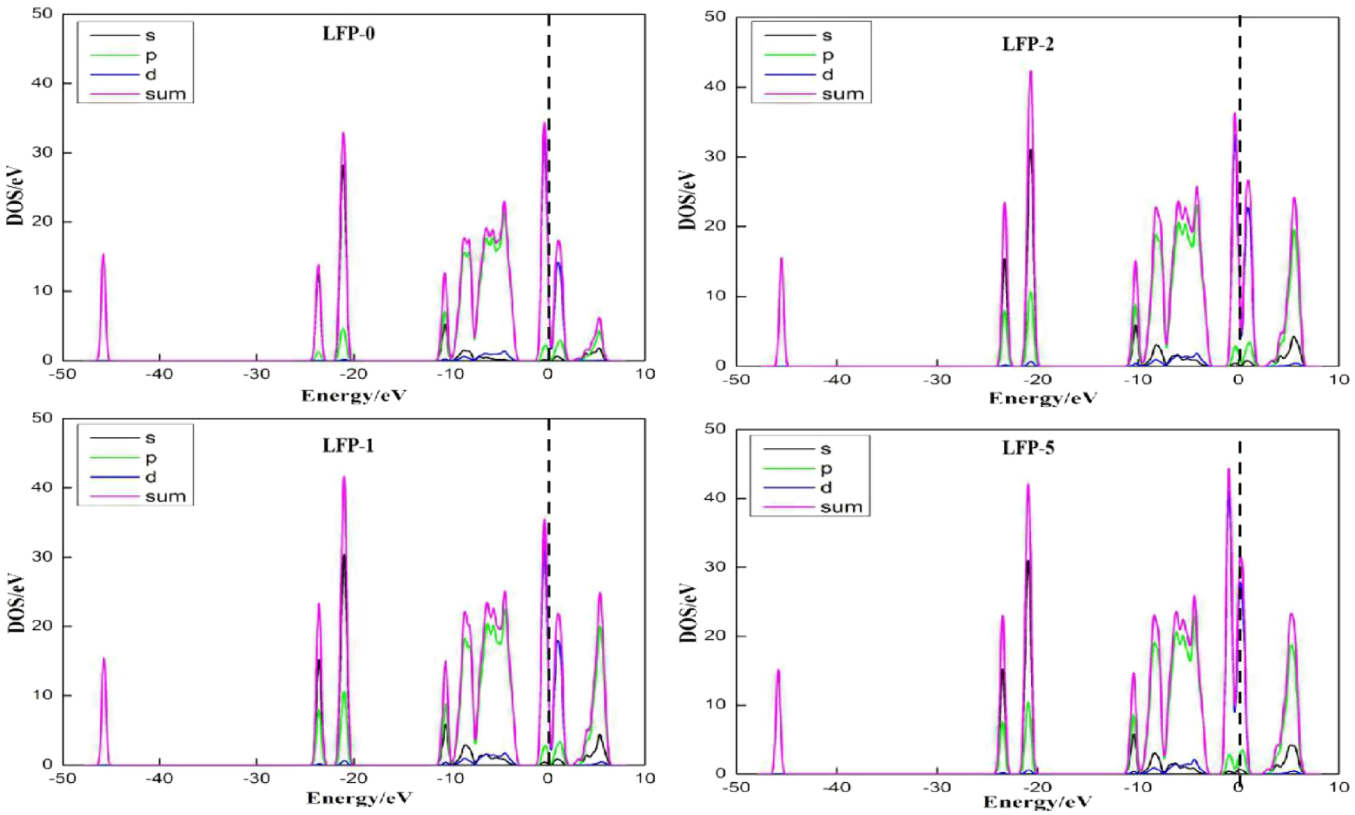


**Figure 3.** Density of state (DOS) of $LiFe_{1-x}Ru_xPO_4$ ($x$ = 0, 0.01, 0.02, and 0.05) and element density of states.

0.01) cathode also displayed a satisfactory cycle life. Figure 5 shows that the LFP-1 ($x$ = 0.01) cathode still retained 95.6% of its initial capacity after 300 cycles at 5 C. Combined with the previous theoretical calculation, we believe outstanding rate



https://doi.org/10.1021/acsomega.1c00595
ACS Omega 2021, 6, 14122−14129

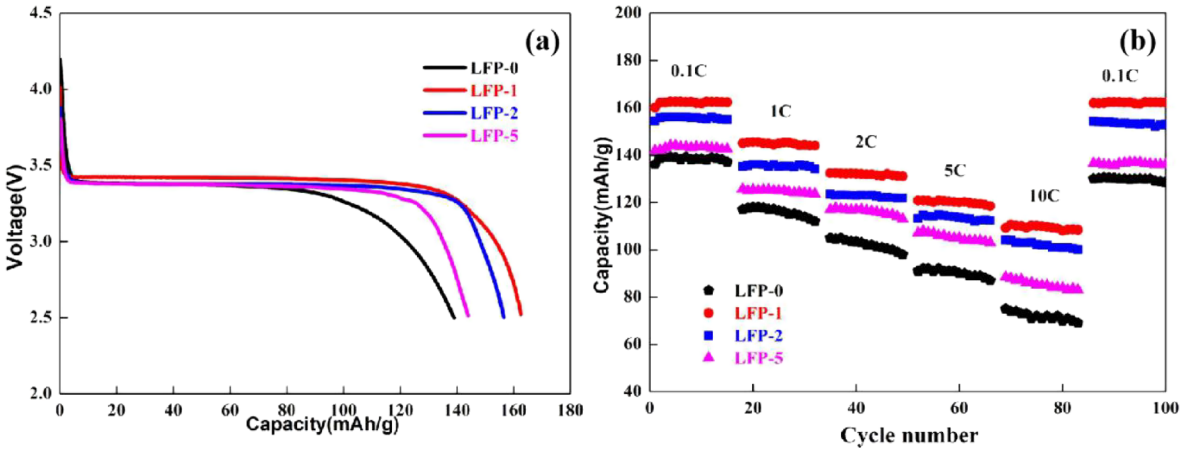


**Figure 4.** (a) First discharge curves of Ru-doped $LiFe_{1-x}Ru_xPO_4/C$ electrodes with different contents at a low rate (0.1 C) and (b) rate capability of $LiFe_{1-x}Ru_xPO_4/C$ electrodes at various rates.

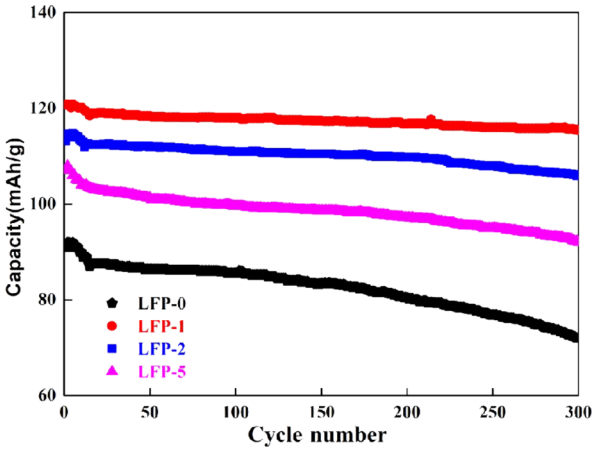


**Figure 5.** Cycling performance of $LiFe_{1-x}Ru_xPO_4/C$ samples at 5 C after 300 cycles.

capabilities and cycle performance of LFP-1 are attributed to proper heteroatom Ru doping in $LiFePO_4$, consistent with our theoretical understanding described above.

To further investigate the effect of Ru doping on the Li-ion diffusion coefficient of $LiFePO_4$, electrochemical impedance spectra of the assembled half cells were measured. The equivalent circuit and Nyquist diagram of $LiFe_{1-x}Ru_xPO_4/C$ composite cathode materials after 3 cycles under full charge are presented in Figure 6a. All the curves are composed of two parts, one is a semicircle in high-frequency regions, and the other is inclined lines in low-frequency regions, corresponding to the double-layer response at the electrode interface and the diffusion of lithium ions in the solid phase.[31] Ohmic resistance ($R_\Omega$), constant-phase element ($C_{dl}$), charge transfer ($R_{ct}$), and the Warburg impedance ($Z_w$) constitute an equivalent circuit pattern. The relationship graph between $Z'$ and $\omega^{-1/2}$ shows a slope of $\sigma$ linear relationship in Figure 6b.

The lithium diffusion coefficient ($D_{Li}^+$) of the $LiFePO_4$ electrode material is counted based on the following formulas (eqs 1 and 2).[32,33]

$$D^+_{Li} = \frac{R^2T^2}{2A^2n^4F^4C_{Li}^2\sigma^2} \quad (1)$$

$$Z' = R_\Omega + R_{ct} + \sigma\omega^{-1/2} \quad (2)$$

Table 2 shows EIS results of the $LiFe_{1-x}Ru_xPO_4/C$ with different Ru amounts after 3 cycles. The diffusion coefficients of lithium ions ($D_{Li}^+$) of samples are $3.64 \times 10^{-12}$, $1.11 \times 10^{-11}$, $8.64 \times 10^{-12}$, and $6.08 \times 10^{-12}$ $cm^2\ s^{-1}$ separately. Apparently, Ru-doped samples have a higher lithium-ion diffusion coefficient. LFP-1 ($x$ = 0.01) exhibits the highest $Li^+$ diffusion coefficient ($1.11 \times 10^{-11}$ $cm^2\ s^{-1}$) and the lowest

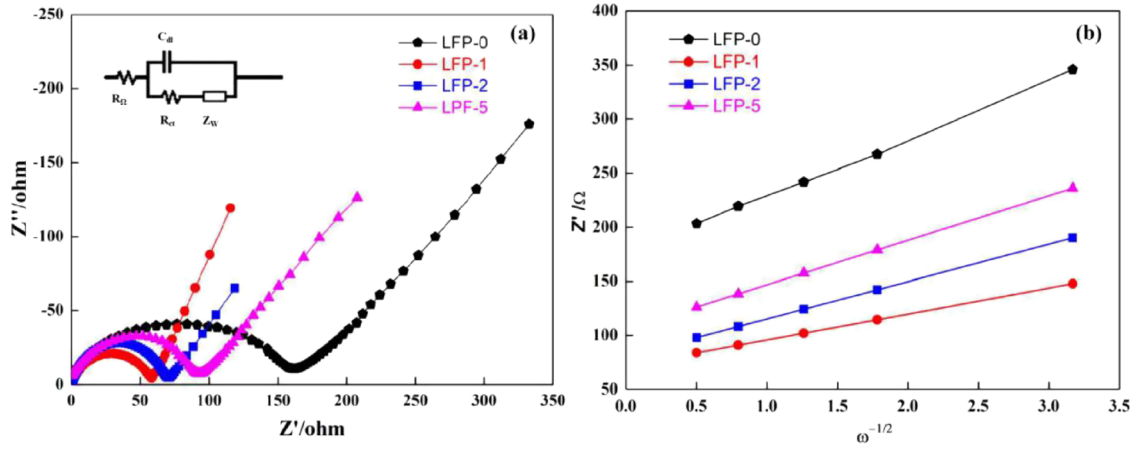


**Figure 6.** (a) Electrochemical impedance spectra of $LiFe_{1-x}Ru_xPO_4/C$ and (b) $Z'$ and $\omega^{-1/2}$ linear relationship in the low-frequency region.



https://doi.org/10.1021/acsomega.1c00595
ACS Omega 2021, 6, 14122−14129

**Table 2. EIS Results and $D_{Li}^{+}$ of $LiFe_{1-x}Ru_xPO_4/C$ ($x$ = 0, 0.01, 0.02, and 0.05) Electrodes**

| sample | $R_\Omega$ (Ω) | $R_{ct}$ (Ω) | $\sigma$ (s cm$^{-1}$) | $D_{Li}$ (cm$^2$ s$^{-1}$) |
|---|---|---|---|---|
| LFP-0 | 0.51 | 161.87 | 53.25 | $3.64 \times 10^{-12}$ |
| LFP-1 | 0.55 | 58.40 | 30.47 | $1.11 \times 10^{-11}$ |
| LFP-2 | 0.58 | 70.26 | 34.57 | $8.64 \times 10^{-12}$ |
| LFP-5 | 0.63 | 92.93 | 41.21 | $6.08 \times 10^{-12}$ |

charge transfer resistance (58.40 Ω) at the same temperature. The EIS results clearly indicate that appropriate Ru doping can enhance $Li^+$ mobility in the bulk of the olivine structure and reduce the resistance in the cathode electrolyte interface, resulting in improved electrochemical activity of $LiFePO_4$. When the doping amount of Ru is further increased, Ru will occupy both Li and Fe sites, which will block the $Li^+$ diffusion channel.

**2.3. SEM, Element Mapping, and XPS Analysis.** Morphologies of LFP-0 and LFP-1 were characterized using a field emission scanning electron microscope (FE-SEM). The powder is composed of small secondary particles with regular dispersion. It is interesting to notice that LFP-1 powders (Figure 7b,d) show uniform submicrometer-sized smaller primary nanoparticles (50−200 nm) connected to each other to compose a porous structure with less aggregates than LFP-0 powders (Figure 7a,c). This may be attributed to the fact that Ru doping can promote the nucleation process and effectively inhibit the particle growth at high temperature.[34,35] The finer particle size and better dispersion can reduce the diffusion path of $Li^+$ and provide a larger surface for $Li^+$ extraction/insertion, resulting in its enhanced diffusion speed. The energy-dispersive

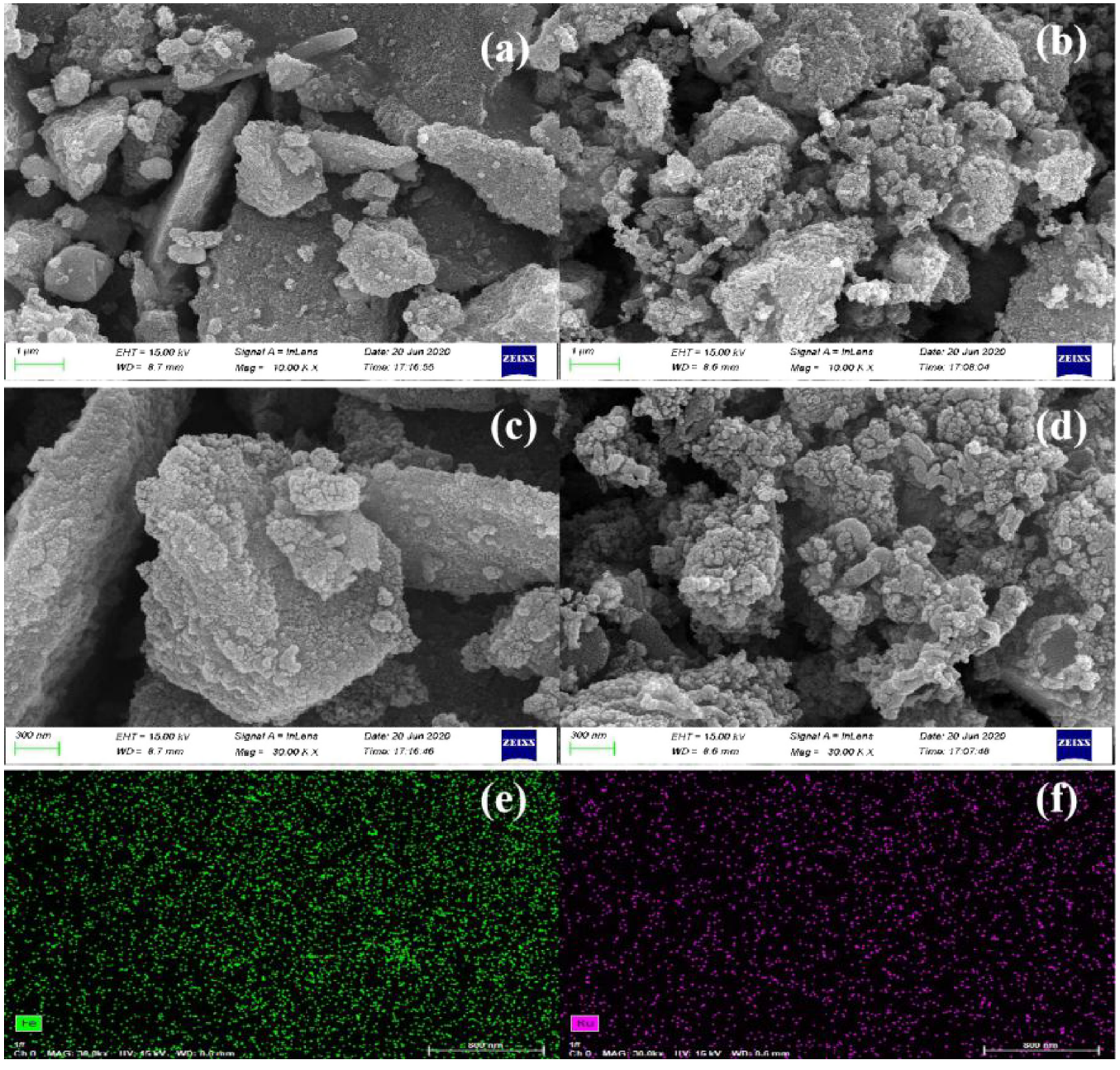


**Figure 7.** SEM images of LFP-0 (a,c) and LFP-1 (b,d) and (e,f) EDX elemental mapping images of Fe and Ru.


https://doi.org/10.1021/acsomega.1c00595
ACS Omega 2021, 6, 14122−14129

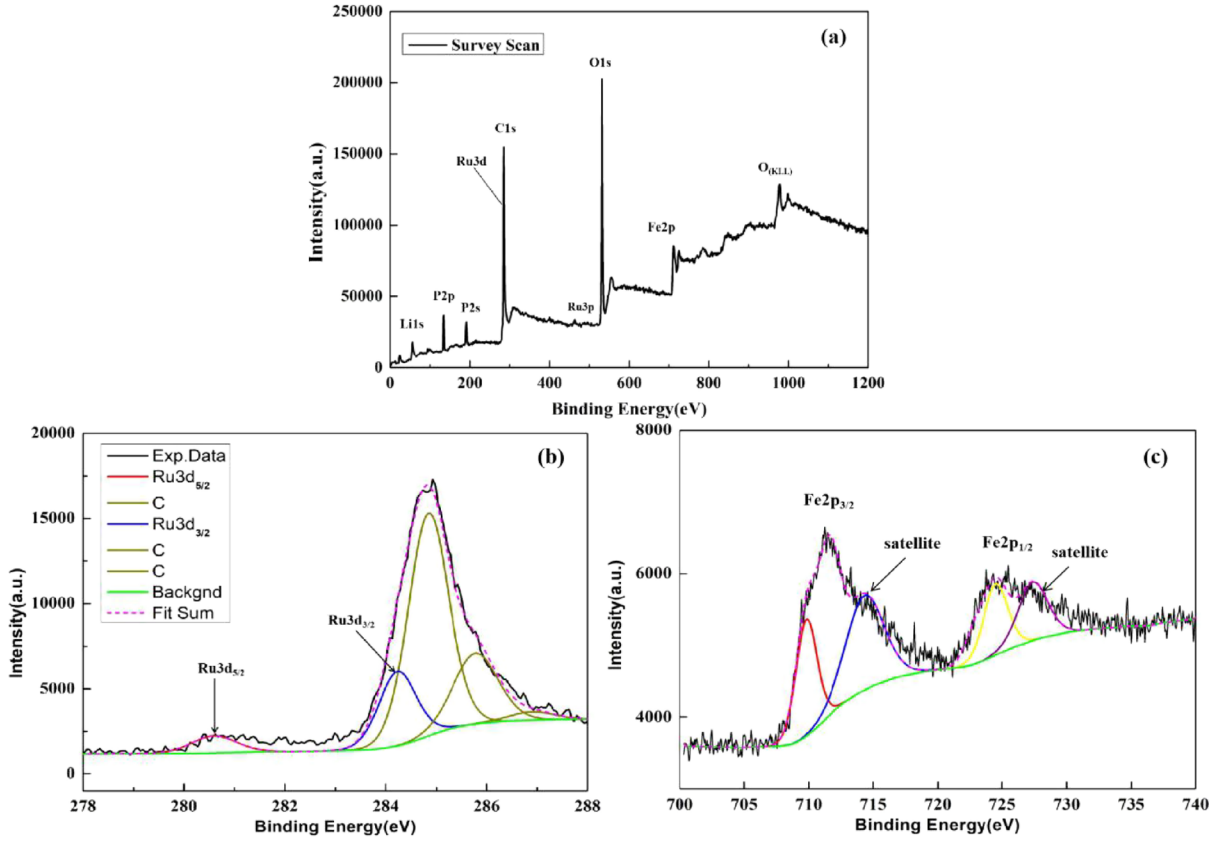


**Figure 8.** (a) Survey X-ray photoelectron spectra for LFP-1 as well as the deconvoluted peaks of (b) Ru 3d and (c) Fe 2p.

X-ray (EDX) elemental mapping images of LFP-1 are shown in Figure 7e,f. The results indicate that Fe and Ru elements have monotonous dispersion, and Ru was doped into the lattice of bulk materials.

In order to better understand the valence of Ru, LFP-1 was characterized by XPS, and the results are shown in Figure 8. Figure 8a shows the survey scan of the LFP-1 depicting the presence of the expected core levels of Li 1s, Fe 2p, Ru 3d, P 2p, C 1s, and O 1s. As seen in Figure 8b, the high-resolution Ru 3d XPS spectrum shows that the spin−orbit is divided into $3d_{5/2}$ and $3d_{3/2}$ peaks, although it is hard to discriminate the Ru 3d peak from the carbon peak. The centers of the two split peaks are 280.7 and 284.4 eV, corresponding to Ru $3d_{5/2}$ and Ru $3d_{3/2}$, respectively. According to previous research,[36] it can be inferred that Ru has +4 valence. Figure 8c shows the Fe 2p spectra, and as a result of the effect of spin−orbit coupling, the spectrum of Fe 2p is divided into two peaks, corresponding to Fe $2p_{3/2}$ and Fe $2p_{1/2}$.[37] One peak is Fe $2p_{3/2}$, which is composed of the main peak of 709.8 eV and a satellite peak of 714.7 eV. The other peak is Fe $2p_{1/2}$, which is composed of the main peak of 724 eV and a satellite peak of 727.4 eV.[38] According to the XPS results, it can be inferred that Fe exists in LFP-1 with +2 valence.[38] The $Ru^{4+}$ heteroatom substitutes for $Fe^{2+}$, in which case, Fe or Li vacancies will be formed in the $LiFePO_4$ lattice to supplement the charge after doping. Charge compensation might promote the ability of $Li^+$ transmission in the bulk phase and improve the electrochemical performance of $LiFePO_4$.

## 3. EXPERIMENTAL SECTION

**3.1. Calculation Methods.** In the theoretical calculations, the first-principles calculation, which is based on density functional theory (DFT), was run in the CASTEP of Materials Studio software 8.0 using an ultrasoft pseudopotential (USPP) method.[39] In terms of the electronic exchange-correlation functional, Fe d orbitals are modified by GGA+$U$ ($U$ = 4.6 eV, $J$ = 0), which makes the calculated band gap of $LiFePO_4$ consistent with the experimental value.[40] An appropriate $k$-point mesh (3×3×3) was chosen to ensure that the total energies converge within $1.0 \times 10^{-4}$ eV·atom$^{-1}$. Three hundred electronvolts was chosen as the cutoff energy.

$LiFePO_4$ is a typical olivine-type structure, and the cell parameters of $LiFePO_4$ are $a$ = 10.3297 Å, $b$ = 6.0115 Å, $c$ = 4.7017 Å, and $\alpha = \beta = \gamma = 90°$.[41,42] After optimizing the structure of $LiFePO_4$, a bulk model of Ru-doped $LiFePO_4$ is shown in Figure 9.

**3.2. Synthesis.** Ru-doped $LiFe_{1-x}Ru_xPO_4/C$ ($x$ = 0, 0.01, 0.02, and 0.05) were synthesized by a sol−gel preparation route from a mixture of stoichiometric amounts of reagents $CH_3CO_2Li{\cdot}2H_2O$, $Fe(NO_3)_3{\cdot}9H_2O$, $H_3PO_4$, $RuCl_3$, and citric acid. The synthesis details of Ru-doped $LiFePO_4/C$ are similar to those of our previous studies.[43] $LiFe_{1-x}Ru_xPO_4/C$ samples are named as LFP-0 ($x$ = 0), LFP-1 ($x$ = 0.01), LFP-2 ($x$ = 0.02), and LFP-5 ($x$ = 0.05).

**3.3. Materials Characterization.** X-ray diffraction (XRD, MO3xHF22, MacScience, Japan) was employed to characterize the crystal structure of $LiFe_{1-x}Ru_xPO_4/C$ under the conditions of Cu K$\alpha$ radiation and a speed of 1 °C/min.

A scanning electron microscope (SEM, Zeiss SIGMA 500, Germany) was used for analysis of material morphology. X-ray


https://doi.org/10.1021/acsomega.1c00595
ACS Omega 2021, 6, 14122−14129

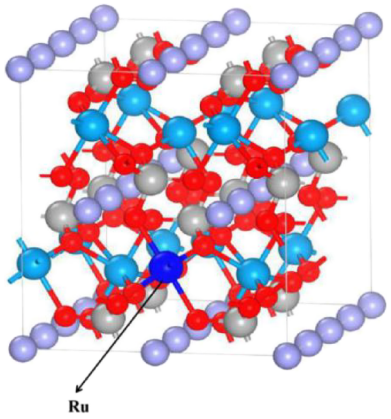


**Figure 9.** Cell structure model of Ru-doped $LiFePO_4$.

photoelectron spectroscopy (XPS; Thermo VG Scientific Co., Ltd.) was applied to analyze the valence states of elements in the $LiFe_{1-x}Ru_xPO_4/C$.

**3.4. Electrochemical Measurements.** The charge and discharge performances were tested using a Neware BTS-5V3A automatic battery tester between 2.5 and 4.2 V (vs Li /$Li^+$). An electrochemical workstation (Solartron, 1287+1260) was employed to perform electrochemical impedance spectroscopy (EIS) at the potential amplitude of 5 mV and the frequency range of $10^{-2}$−$10^5$ Hz.

For electrochemical characterization, cathodes of 85 wt % $LiFe_{1-x}Ru_xPO_4/C$, 6 wt % ethyne black, and a 9 wt % PVDF binder distributed throughout *N*-methylpyrrolidone were made and coated on an Al substrate current collector. Cathodes were dried in vacuum at 80 °C for 24 h. CR2016-type coin cells were packaged in an Ar glovebox. A lithium metal was used as a counter electrode, $LiPF_6$ in a mixture solvent (DMC:EC = 50:50 vol %) was employed as an electrolyte, and PP (Celgard 2300) was used as a diaphragm.

## 4. CONCLUSIONS

In this study, with united use of the first-principles theoretical calculation method, experiments, and characterization, the results suggested that ruthenium doping occupying iron sites leads to a significantly improved lithium diffusion coefficient and electrical conductivity, therefore strongly increasing electrochemical performance. LFP-1 ($x$ = 0.01) delivers excellent specific capacities of 162.6 and 110.6 mA h $g^{-1}$ at 0.1 and 10 C and at the same time displays good cycle life. Ru doping will affect the electronic structure of $LiFePO_4$, resulting in the shortening of $Li^+$ diffusion distance, the increase in Fermi energy, and the reduction in the band gap. In addition, it is also conducive to promote electron and $Li^+$ transport. Such a concept of doping substitution can be extended to optimize the specific capacity and rate capability of other materials with poor conductivity.

## AUTHOR INFORMATION


### Corresponding Authors

**Yuan Gao** − *School of Environment and Resources, Engineering Research Center for Waste Oil Recovery Technology and Equipment of Ministry of Education, Chongqing Technology and Business University, Chongqing 400067, People's Republic of China*; Email: gaogone113117@ctbu.edu.cn

**Bingfeng Zhu** − *The First Affiliated Hospital of Chongqing Medical and Pharmaceutical College, Chongqing 400040, People's Republic of China*; Email: 2621266253@qq.com

### Authors

**Kun Xiong** − *School of Environment and Resources, Engineering Research Center for Waste Oil Recovery Technology and Equipment of Ministry of Education, Chongqing Technology and Business University, Chongqing 400067, People's Republic of China*; orcid.org/0000-0002-0625-7195

**Haidong Zhang** − *School of Environment and Resources, Engineering Research Center for Waste Oil Recovery Technology and Equipment of Ministry of Education, Chongqing Technology and Business University, Chongqing 400067, People's Republic of China*

Complete contact information is available at: https://pubs.acs.org/10.1021/acsomega.1c00595


### Author Contributions

This manuscript contains works and contributions of all the authors. All authors have read the full text and agreed to publish the manuscript.

### Notes

The authors declare no competing financial interest.

## ACKNOWLEDGMENTS

This research was funded by the Scientific and Technological Projects from Chongqing Education Commission (KJQN2019008832), the School Science Fund Projects from Chongqing Technology and Business University (1856022), and the Research platform open project of Chongqing Technology and Business University (KFJJ2019086).

## REFERENCES


(1) Padhi, A. K.; Nanjundaswamy, K. S.; Goodenough, J. B. Phospho-olivines as positive-electrode materials for rechargeable lithium batteries. *J. Electrochem. Soc.* **1997**, *144*, 1188−1194.

(2) Alias, N.; Mohamad, A. A. Advances of aqueous rechargeable lithium-ion battery: a Review. *J. Power Sources* **2015**, *274*, 237−251.

(3) Chung, S.-Y.; Bloking, J. T.; Chiang, Y.-M. Electronically conductive phospho-olivines as lithium storage electrodes. *Nat. Mater.* **2002**, *1*, 123−128.

(4) Armand, M.; Tarascon, J. M. Building better batteries. *Nature* **2008**, *451*, 652−657.

(5) Huang, S.; Ren, J.; Liu, R.; Bai, Y.; Li, X.; Huang, Y.; Yue, M.; He, X.; Yuan, G. Enhanced electrochemical properties of $LiFePO_4$ cathode using waterborne lithiated ionomer binder in Li-ion batteries with low amount. *ACS Sustainable Chem. Eng.* **2018**, *6*, 12650−12657.

(6) Sun, X.; Li, J.; Shi, C.; Wang, Z.; Liu, E.; He, C.; Du, X.; Zhao, N. Enhanced electrochemical performance of $LiFePO_4$ cathode with in-situ chemical vapor deposition synthesized carbon nanotubes as conductor. *J. Power Sources* **2012**, *220*, 264−268.

(7) Gowneni, S.; Basak, P. Swapping conventional salts with an entrapped lithiated anionic polymer: fast single-ion conduction and electrolyte feasibility in $LiFePO_4$/Li batteries. *J. Mater. Chem. A* **2017**, *5*, 12202−12215.

(8) Guo, X.; Lan, T.; Zhang, L.; Tan, J.; Feng, X.; Chen, L. Y. A stable filamentous coaxial microelectrode for Li-ion batteries: a case of olivine $LiFePO_4$. *Chem. Commun.* **2019**, *55*, 3529−3531.

(9) Saikia, D.; Deka, J. R.; Chou, C. J.; Lin, C. H.; Yang, Y. C.; Kao, H. M. Encapsulation of $LiFePO_4$ Nanoparticles into 3D Interpenetrating Ordered Mesoporous Carbon as a High-Performance Cathode for Lithium-Ion Batteries Exceeding Theoretical Capacity. *ACS Appl. Energy Mater.* **2019**, *2*, 1121−1133.

(10) Tian, H.; Zhao, X.; Zhang, J.; Li, M.; Lu, H. $LiFePO_4$ Anchored on Pristine Graphene for Ultrafast Lithium Battery. *ACS Appl. Energy Mater.* **2018**, *1*, 3497−3504.
(11) Paolella, A.; Bertoni, G.; Hovington, P.; Feng, Z.; Flacau, R.; Prato, M.; Colombo, M.; Marras, S.; Manna, L.; Turner, S.; Van Tendeloo, G.; Guerfi, A.; Demopoulos, G. P.; Zaghib, K. Cation Exchange mediated elimination of the Fe-antisites in the hydrothermal synthesis of $LiFePO_4$. *Nano Energy* **2015**, *16*, 256−267.
(12) Gao, C.; Zhou, J.; Liu, G.; Wang, L. Synthesis of F-doped $LiFePO_4$/C cathode materials for high performance lithium-ion batteries using co-precipitation method with hydrofluoric acid source. *J. Alloys Compd.* **2017**, *727*, 501−513.
(13) Yang, W.; Chen, Y.; Peng, X.; Lin, Y.; Li, J.; Hong, Z.; Xu, G.; Huang, Z. Enhanced electrochemical performances of Cu/$Cu_xO$ composite decorated $LiFePO_4$ through a facile magnetron sputtering. *ACS Appl. Energy Mater.* **2019**, *2*, 4652−4663.
(14) Yang, C.-C.; Hsu, Y.-H.; Shih, J.-Y.; Wu, Y.-S.; Karuppiah, C.; Liou, T.-H.; Lue, S. J. Preparation of 3D micro/mesoporous $LiFePO_4$ composite wrapping with porous graphene oxide for high-power lithium ion battery. *Electrochim. Acta* **2017**, *258*, 773−785.
(15) Wang, C.; Guo, Z.; Shen, W.; Xu, Q.; Liu, H.; Wang, Y. B-doped carbon coating improves the electrochemical performance of electrode materials for Li-ion batteries. *Adv. Funct. Mater.* **2014**, *24*, 5511−5521.
(16) Nan, C.; Lu, J.; Li, L.; Li, L.; Peng, Q.; Li, Y. Size and shape control of $LiFePO_4$ nanocrystals for better lithium ion battery cathode materials. *Nano Res.* **2013**, *6*, 469−477.
(17) Di Lecce, D.; Gancitano, V.; Hassoun, J. Investigation of Mn and Fe substitution effects on the characteristics of high-Voltage $LiCo_{1-x}M_xPO_4$ ($x$ = 0.1, 0.4) cathodes prepared by Sol−gel route. *ACS Sustainable Chem. Eng.* **2020**, *8*, 278−289.
(18) Lv, Y. J.; Huang, B.; Tan, J. X.; Jiang, S. Q.; Zhang, S. F.; Wen, Y. X. Enhanced low temperature electrochemical performances of $LiFePO_4$/C by $V^{3+}$ and F co-doping. *Mater. Lett.* **2018**, *229*, 349−352.
(19) Shi, S.; Liu, L.; Wang, D.-s.; Wang, Z.; Chen, L.; Huang, X. First-principles investigation of the structural magnetic, and electronic properties of olivine $LiFePO_4$. *Phys. Rev. B* **2005**, *71*, 144404−195112.
(20) Yan, Z.; Huang, D.; Lai, J.; Chu, Y.; Zheng, F.; Cai, Y.; Pan, Q.; Wang, H.; Huang, Y.; Li, Q. Nickel catalyzed graphitized carbon coated $LiFe_{1-x}Ni_xPO_4$ composites as cathode material for high-performance lithium-ion batteries. *Electrochim. Acta* **2020**, *353*, 136565.
(21) Zhang, Y.; Alarco, J. A.; Nerkar, J. Y.; Best, A. S.; Snook, G. A.; Talbot, P. C.; Cowie, B. C. C. Observation of Preferential Cation Doping on the Surface of $LiFePO_4$ Particles and Its Effffect on Properties. *ACS Appl. Energy Mater.* **2020**, *3*, 9158−9167.
(22) Wang, L.; Zhou, F.; Meng, Y.-S.; Ceder, G. First-principles study of surface properties of $LiFePO_4$: Surface energy, structure, Wulff shape, and surface redox potential. *Phys. Rev. B* **2007**, *76*, 165435−165440.
(23) Nanda, J.; Martha, S. K.; Porter, W. D.; Wang, H.; Dudney, N. J.; Radin, M. D.; Siegel, D. J. Thermophysical properties of $LiFePO_4$ cathodes with carbonized pitch coatings and organic binders: Experiments and first-principles modeling. *J. Power Sources* **2014**, *251*, 8−13.
(24) Kou, X.-J.; Ke, H.; Zhu, C.-B.; Rolfe, P. First-principles study of the chemical bonding and conduction behavior of $LiFePO_4$. *Chem. Phys.* **2015**, *446*, 1−6.
(25) Fang, C.-M.; Wijs, G.-A.; Loong, C.-K. Lattice and local-mode vibrations in anhydrous and protonized $LiMn_2O_4$ spinels from first-principles theory. *J. Mater. Chem.* **2017**, *17*, 4908−4913.
(26) Ban, C.; Yin, W.-J.; Tang, H.; Wei, S.-H.; Yan, Y.; Dillon, A. C. A novel Codoping approach for enhancing the performance of $LiFePO_4$ cathodes. *Adv. Energy Mater.* **2012**, *2*, 1028−1032.
(27) Chen, T. C.; Lin, R. H. Effects of Metal doping on properties of $LiFePO_4$ cathode material by First-Principle calculation. *Int. J. Mater. Eng.* **2015**, *5*, 121−124.
(28) Zhang, D.; Zhang, P.; Yi, J.; Yuan, Q.; Jiang, J.; Xu, Q.; Luo, Z.; Ren, X. XRD simulation study of doped $LiFePO_4$. *J. Alloys Compd.* **2011**, *509*, 1206−1210.
(29) Yin, X.; Huang, K.; Liu, S.; Wang, H.; Wang, H. Preparation and characterization of Na-doped $LiFePO_4$/C composites as cathode materials for lithium-ion batteries. *J. Power Sources* **2010**, *195*, 4308−4312.
(30) Shi, S.; Ouyang, C.; Lei, M.; Tang, W. Effect of Mg-doping on the structural and electronic properties of $LiCoO_2$: A first-principles investigation. *J. Power Sources* **2007**, *171*, 908−912.
(31) Liao, X.-Z.; Ma, Z.-F.; Gong, Q.; He, Y.-S.; Pei, L.; Zeng, L.-J. Low-temperature performance of $LiFePO_4$/C cathode in a quaternary carbonate-based electrolyte. *Electrochem. Commun.* **2008**, *10*, 691−694.
(32) Bard, A.J.; Faulkner, L.R. *Electrochemical methods: Fundamentals and applications*; Wiley: New York, 1980; pp. 231−265.
(33) Shu, H.; Wang, X.; Wu, Q.; Liu, L.; Liang, Q.; Yang, S.; Ju, B.; Yang, X.; Zhang, X.; Wang, Y.; Wei, Q.; Hu, B.; Liao, Y.; Jiang, H. The effect of ammonia concentration on the morphology and electrochemical properties of $LiFePO_4$ synthesized by ammonia assisted hydrothermal route. *Electrochim. Acta* **2012**, *76*, 120−129.
(34) Hu, Y.; Yao, J.; Zhao, Z.; Zhu, M.; Li, Y.; Jin, H.; Zhao, H.; Wang, J. ZnO-doped $LiFePO_4$ cathode material for lithium-ion battery fabricated by hydrothermal method. *Mater. Chem. Phys.* **2013**, *141*, 835−841.
(35) Dominko, R.; Bele, M.; Gaberscek, M.; Remskar, M.; Hanzel, D.; Goupil, J. M.; Pejovnik, S.; Jamnik, J. Porous olivine composites synthesized by sol-gel technique. *J. Power Sources* **2006**, *153*, 274−280.
(36) Kim, K. H.; Kim, K. S.; Kim, G. P.; Baeck, S. H. Electrodeposition of mesoporous ruthenium oxide using an aqueous mixture of CTAB and SDS as a templating agent. *Curr. Appl. Phys.* **2012**, *12*, 36−39.
(37) Bhuvaneswari, M. S.; Bramnik, N. N.; Ensling, D.; Ehrenberg, H.; Jaegermann, W. Synthesis and characterization of carbon nano fiber/$LiFePO_4$ composites for Li ion batteries. *J. Power Sources* **2006**, *180*, 553−560.
(38) Castro, L.; Dedryvère, R.; el Khalififi, M.; Lippens, P.-E.; Bréger, J.; Tessier, C.; Gonbeau, D. The spin-polarized electronic structure of $LiFePO_4$ and $FePO_4$ evidenced by in-Lab XPS. *J. Phys. Chem. C* **2010**, *114*, 17995−18000.
(39) Perdew, J. P.; Chevary, J. A.; Vosko, S. H.; Jackson, K. A.; Pederson, M. R.; Singh, D. J.; Fiolhais, C. Atoms, molecules, solids, and surfaces: applications of the generalized gradient approximation for exchange and correlation. *Phys. Rev. B* **1992**, *46*, 6671−6687.
(40) Zhang, H.; Tang, Y.; Shen, J.; Xin, X.; Cui, L.; Chen, L.; Ouyang, C.; Shi, S.; Chen, L. Antisite defects and Mg doping in $LiFePO_4$: a first-principles investigation. *Appl. Phys. A: Mater. Sci. Process.* **2011**, *104*, 529−537.
(41) Kohn, W. Nobel Lecture: Electronic structure of matter-wave functions and density functionals. *Rev. Mod. Phys.* **1999**, *71*, 1253−1266.
(42) Andersson, A. S.; Kalska, B.; Häggström, L.; Thomas, J. O. Lithium extraction/insertion in $LiFePO_4$: an X-ray diffraction and Mössbauer spectroscopy study. *Solid State Ionics* **2000**, *130*, 41−52.
(43) Gao, Y.; Li, L.; Peng, H.; Wei, Z.-D. Surfactant-assisted Sol−Gel synthesis of nanostructured Ruthenium-doped Lithium Iron Phosphate as a cathode for Lithium-ion batteries. *ChemElectroChem* **2014**, *12*, 2146−2152.


https://doi.org/10.1021/acsomega.1c00595
*ACS Omega* 2021, 6, 14122−14129